Highly Efficient Field Emission from Carbon Nanotube−Nanohorn Hybrids Prepared by Chemical Vapor Deposition

Ryota Yuge,[†,*] Jin Miyawaki,[‡,#] Toshinari Ichihashi,[†] Sadanori Kuroshima,[†] Tsutomu Yoshitake,[†] Tetsuya Ohkawa,[§] Yasushi Aoki,[§] Sumio Iijima,[†,⊥] and Masako Yudasaka[†,‡,¶,*]

[†]Green Innovation Research Laboratories, NEC Corporation, 34 Miyukigaoka, Tsukuba 305-8501, Japan, [‡]Japan Science and Technology Agency, Sanbancho Bldg., 5, Sanbancho Chiyoda-ku, Tokyo 102-0075, Japan, [§]Research and Development Department, NEC Lighting, Ltd., 3-1 Nichiden, Minakuchi, Koga, 528-8501, Japan, [⊥]Department of Materials Science and Engineering, Meijo University, 1-501 Shiogamaguchi, Nagoya 468-8502, Japan, and [¶]Nanotube Research Center, National Institute of Advanced Science and Technology (AIST), Central 5, 1-1-1 Higashi, Tsukuba, 305-8565, Japan. [#]Present address: Institute for Materials Chemistry and Engineering, Kyushu University, 6-1 Kasugakoen, Kasuga, Fukuoka, 816-8580, Japan.

ABSTRACT Electrically conductive carbon nanotubes (CNTs) with high aspect ratios emit electrons at low electric fields, thus applications to large-area field emission (FE) devices with CNT cathodes are attractive to save energy consumption. However, the poor dispersion and easy bundling properties of CNTs in solvents have hindered this progress. We have solved these problems by growing single-walled CNTs (SWNTs) on single-walled carbon nanohorn (SWNH) aggregates that have spherical forms with *ca.* 100-nm diameters. In the obtained SWNT−SWNH hybrids (NTNHs), the SWNTs diameters were 1−1.7 nm and the bundle diameters became almost uniform, that is, less than 10 nm, since the SWNTs were separated by SWNH aggregates. We also confirmed that a large-area FE device with NTNH cathodes made by screen printing was highly and homogeneously bright, suggesting the success of the hybrid strategy.

KEYWORDS: carbon nanotube · carbon nanohorn · single-walled carbon nanotube · single-walled carbon nanohorn · chemical vapor deposition · field emission

Single-walled carbon nanotubes (SWNTs)[1,2] have gathered much attention from both academic and industrial researchers due to their unique physical and chemical properties. Potential applications of SWNTs include electronic devices,[3−5] sensing applications,[6,7] super strong engineering fibers,[8,9] and catalyst supports.[10,11] The electrically conductive SWNTs with high aspect ratio can emit electrons at low electric field, thus field emission displays (FEDs)[12,13] and field emission lamps (FELs)[14,15] with SWNT cathodes are eagerly anticipated to cope with energy and environmental problems.

In the fabrication of the carbon nanotube (CNT) cathodes for FEDs and FELs, CNTs are deposited on the substrate by direct growth,[16,17] electrophoresis,[18] or printing.[19,20] For the FEDs or FELs, the simple, scalable, and low-cost method of the printing is appropriate. However, the poor dispersibility of CNTs in solutions due to entanglement and bundling results in inhomogeneous distribution of CNTs in the electrodes, leading to patchy light emission. We considered that the hybridization of SWNTs with electrically conductive nanoparticles dispersing well in the solvents would solve this problem. As such nanoparticles, we used single-walled carbon nanohorns (SWNHs).[21,22] Each SWNH is an irregularly shaped tube made of single-graphene sheets. The diameter of each SWNH was 2 to 5 nm. About 2000 SWNHs assemble to form a spherical aggregate with dahlia-flower-like forms having diameters of 80 to 100 nm. SWNHs disperse well in various solvents (see Supporting Information Figure S1), and have high electrical conductivity.[23,24] Furthermore, SWNHs can be used as a support material to form small sized catalysts on their outer surface and inside internal space.[25,26] Their potential applications as catalyst supports,[25,26] capacitor electrodes,[27] and drug carriers[28,29] in medical fields have also been studied.

In this study, we obtained SWNT−SWNH hybrid (NTNH) by growing SWNTs from Fe catalyst supported on SWNHs by chemical vapor deposition (CVD). Owing to the high dispersibility of the NTNH in the solvents, the NTNHs were homogeneously and sparsely deposited on the electrodes by a simple printing technique. In addition, the SWNT bundles in the NTNHs were thin in comparison with those in usual SWNTs. As a result, evenly and highly bright flat FELs were successfully fabricated using NTNHs as the cathode. We believe that the CNT−nanoparticle hybrid is promising for the development of the CNT−FE technology.

*Address correspondence to r-yuge@bk.jp.nec.com, m-yudasaka@aist.go.jp.

Received for review September 18, 2010 and accepted November 01, 2010.

Published online November 10, 2010. 10.1021/nn102452q

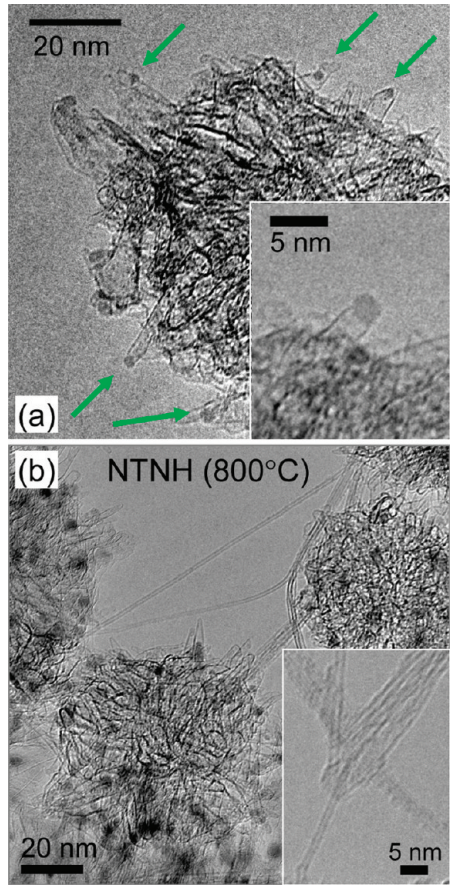

Figure 1. TEM images of Fe@NHoxh (a) and NTNH obtained at 800 °C (b).

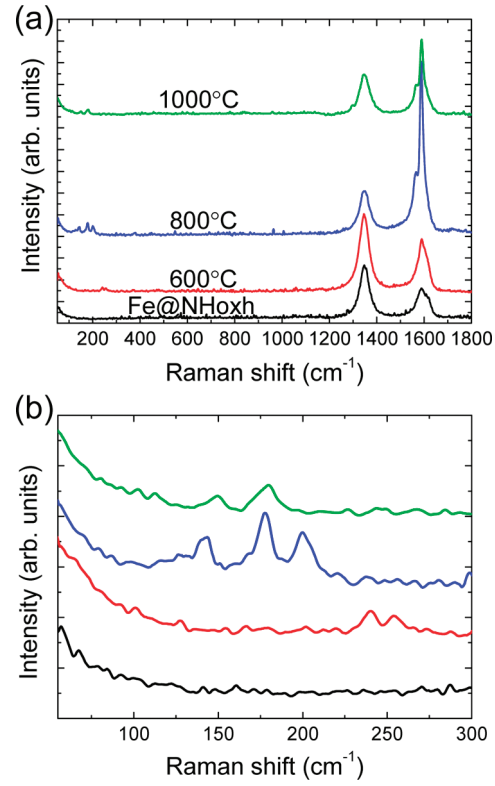

Figure 2. Raman spectra (a) and the enlarged RBM peaks (b) of Fe@NHoxh (black line) and NTNH obtained at 600 (red line), 800 (blue line), and 1000 °C (green line).

RESULTS AND DISCUSSION

The structure of the specimens was first studied by a transmission electron microscope (TEM) observation. The TEM images of Fe@NHoxh (Fe oxide deposited hole-opened SWNH), a starting material of ethanol CVD (Figure 1a),[30−32] showed dark spots of Fe oxide with sizes of 2−4 nm located at the tips (inset in Figure 1a) and outside of the SWNH sheaths. On the other hand, in the TEM images of NTNHs obtained by the ethanol CVD at 800 °C, SWNTs were obviously seen (Figure 1b) and their diameters were about 1 nm (inset in Figure 1b). SWNTs with diameters larger than 2 nm were also sometimes found. The SWNTs in the NTNHs existed individually or formed thin bundles, as apparent from TEM images. The bundle diameters were less than 10 nm (Figure 1b). We did not find any multiwalled carbon nanotubes (MWNTs) in the NTNHs. The TEM images of NTNHs obtained by CVD at 600 and 1000 °C are also shown in Supporting Information Figure S2.

For further structural analysis of the NTNH, we measured the Raman spectra as shown in Figure 2. The Raman spectra of Fe@NHoxh (Figure 2, Table 1) were similar to those of NHox (hole-opened SWNH),[30] exhibiting a broad G band (~1590 cm^{-1}) with a shoulder (1620 cm^{-1}) and a broad D band (~1350 cm^{-1}). The G band originates from the E_{2g} stretching mode of graphite, and the D band reflects the graphite-structure imperfection. The shoulder corresponds to defects of NHox introduced by oxidation at 500 °C for hole-opening.[30] In addition to these peaks, the Raman spectra of the NTNH exhibited that the peaks originated from the SWNTs (Figure 2, Table 1). Especially the NTNH prepared at 800 °C clearly showed the radial breathing modes (RBMs, 100−300 cm^{-1}) and sharp G band (~1589 cm^{-1}), which are characteristic of SWNTs.[33,34] Since the Raman peaks of SWNTs were less clear for NTNH prepared at 600 or 1000 °C, we considered that an optimum SWNT growth temperature for the NTNH preparation by CVD was 800 °C.

The SWNT diameters estimated from the RBM peak positions according to the relationship of $d = 248/\omega$ (d, diameter; ω, peak wavenumber)[34] were 1.0−1.7 nm (Table 1). The diameters increased with the CVD temperature, which is likely because the Fe-particle size increased with the CVD temperature.[35−37] The Raman

TABLE 1. Diameters of SWNTs Estimated from RBM Peaks and Peak Positions of D and G Bands in Raman Spectra

	diameter (nm)	RBM (cm^{-1})	D band (cm^{-1})	G band (cm^{-1})
Fe@NHoxh			1345	1590
NTNH 600 °C	0.98, 1.03	240, 254	1346	1590
NTNH 800 °C	1.24, 1.39, 1.73	200,178, 143	1346	1588
NTNH 1000 °C	1.39, 1.65	179, 150	1347	1589

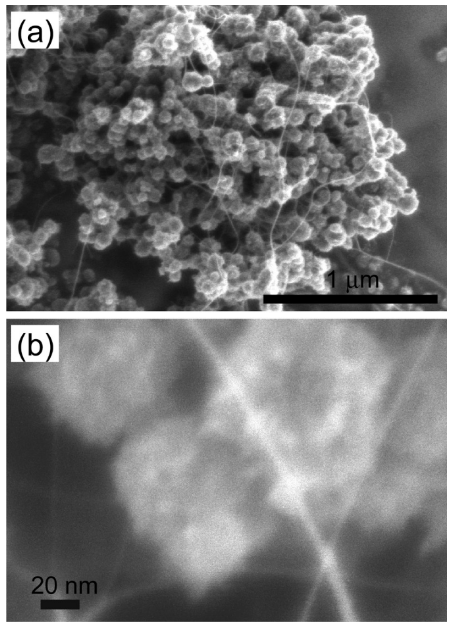

Figure 3. SEM image of NTNH prepared at 800 °C.

peaks corresponding to Fe oxide or other Fe compounds did not appear in the observed spectra.

The overall structure of the NTNH prepared at 800 °C was observed directly with a scanning electron microscope (SEM) (Figure 3). Also, the magnified SEM image in Figure 3b shows bundled SWNTs and Fe@NHoxh after ethanol CVD. Surprisingly, we found that large-bundles did not form easily and bundle diameters became approximately uniform, because the SWNTs were separated by SWNH aggregates (Figure 3). In fact, the bundle diameters of the SWNTs were estimated roughly; about 95% were less than 10 nm (A histogram of diameter distributions of the NTNH was obtained by counting 200 bundles. See Supporting Information Figure S3). We also confirmed that the NTNHs in ethanol were easily monodispersed like SWNH aggregates (see Supporting Information Figure S4), though the particle size became larger, probably due to re-aggregation caused by tangling of the SWNTs on the NTNH.

Next, we investigated Fe-based catalysts of NTNH hybrid after ethanol CVD. Figure 4 shows a Z-contrast image prepared at 800 °C and histograms of the catalyst sizes estimated from about 300 white spots (a scanning transmission electron microscope (STEM) image of NTNH prepared at 800 °C is not shown. See Supporting Information Figure S5). In the Z-contrast image, the Fe particles appear clearly as bright spots (Figure 4a) because the image contrast is proportional to the square of the atomic number. We found that small sizes of Fe-based particles were largely maintained at 600 and 800 °C, although the CVD growth at 1000 °C enlarged the catalysts and caused a wide diameter distribution due to migration and aggregation at high temperatures (Figure 4b).

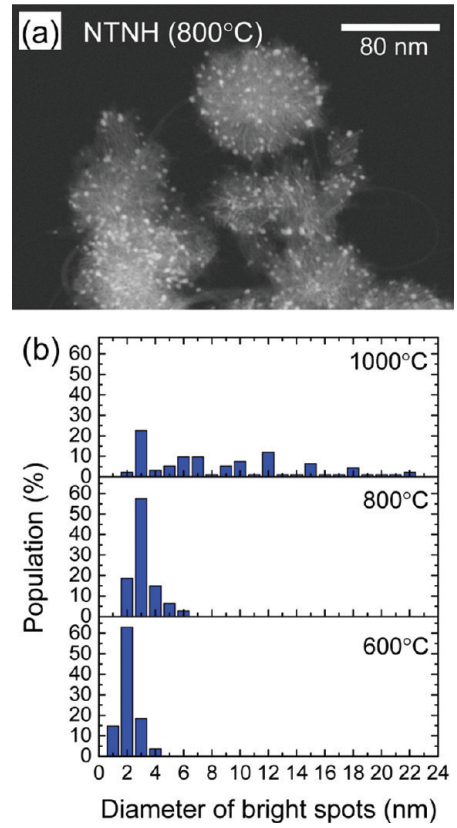

Figure 4. (a) Z-contrast image of NTNH prepared at 800 °C. (b) Histograms of Fe particle sizes in NTNHs after ethanol CVD.

In conclusion, the CVD growth at 800 °C was found to be optimum for the preparation of the NTNH hybrid, and thus we selected NTNH prepared at 800 °C for further FEL study.

The relation of electron emission current density and electric field for the NTNH-FELs showed a turn-on electric field, defined as the electric field value at a current of 1 μA/cm^2, at 5 kV/cm (Figure 5a, black). Here, the emission current density is the emission current per unit electrode area. The turn-on electric field for NTNH-FELs was lower than that for FELs of HiPco-SWNTs, HiPco-SWNTs/SWNHs, and SWNHs (Table 2). The emission current of the NTNH-FELs was higher than that of the other FELs (Figure 5a). It should be noted that the flat FEL devices from all specimens were prepared in the same way, and the FE properties were similarly measured. The reasons the NTNH is so effective were analyzed as follows.

The electron emission from the tips of SWNTs is known to be tunneling-effect emission, and the relationship between the current and electric field follows the Fowler−Nordheim (F−N) relation.[38−40] In this mechanism, the electron emission depends only on the local electric field without a thermal process, therefore it is called cold emission. This type of emission is usually found at high electric fields, about 10^7 V/cm, for the metal electrodes under high vacuum,[39] but it de-

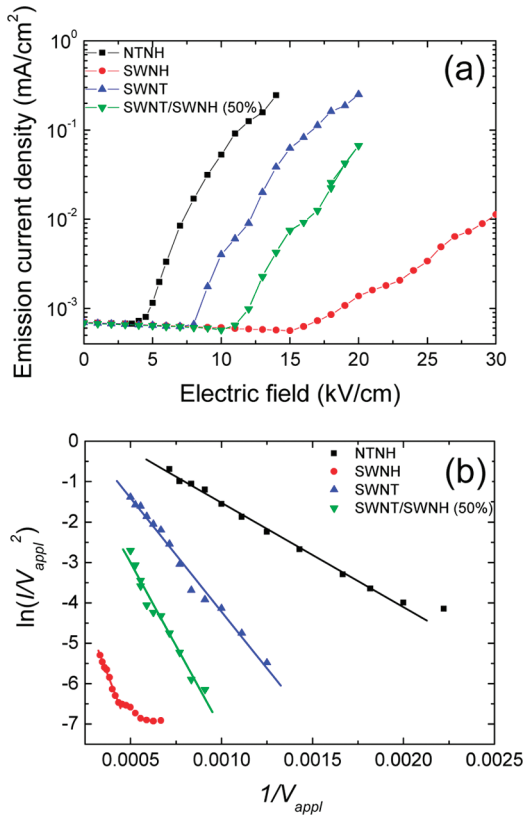

Figure 5. *J*−*E* curves (a) and F−N plots (b) obtained for emitters prepared using NTNHs, SWNHs, HiPco-SWNTs, and HiPco-SWNTs/SWNHs (a mixture of SWNTs and SWNHs), respectively. F−N plots are composed of linear relationships with the slopes of each sample.

creases to the order of 10^3 V/cm for the SWNTs due to the high aspect ratio.[41]

According to the F−N theory, the current, I (A), is given by the following equation.[40]

$$I = S\frac{1.5 \times 10^{-6}(E_{local})^2}{\phi}\exp\left(\frac{10.4}{\sqrt{\phi}}\right)\exp\left(-\frac{6.44 \times 10^7 \phi^{1.5}}{E_{local}}\right) \quad (1)$$

Here, E_{local} (V/cm) is a local electric field at a given emission site and ϕ (eV) is the work function of an emitter material. We assumed ϕ of SWNHs or SWNTs was 5.0 eV,[42,43] which is a typical value for CNTs (SWNT, double-wall carbon nanotube, MWNT, *etc.*). E_{local} was assumed to be proportional to V_{appl}, $E_{local} = \beta V_{appl}$,[38−40] where β (cm^{-1}) is a field enhancement factor and V_{appl} (V) is an applied voltage. Substituting these relations into eq 1, we obtained the following:

$$\ln\left(\frac{I}{V_{appl}^2}\right) = -\frac{6.44 \times 10^7 \times \phi^{1.5}}{\beta}\frac{1}{V_{appl}} + \ln\left(\frac{1.5 \times 10^{-6} \times S\beta^2}{\phi}\exp\left(\frac{10.4}{\sqrt{\phi}}\right)\right) \quad (2)$$

In this equation, S (cm^2) is an effective electron-emission area of the cathode electrode. The $\ln(I/V_{appl}^2)$ and $1/V_{appl}$ have a linear relationship, and the β value corresponds to the slope of the linear line. The value of S is the value of $\ln(I/V_{appl}^2)$ at $1/V_{appl} = 0$. For the CNT emitters, it has been reported that the β values are influenced by tip structures, the radius of the emitter (=bundle diameter), the aspect ratio, and the density of CNTs standing on the substrate.[39,41,44,45]

A cell with specimens on the cathodes showed the linear relations between $\ln(I/V_{appl}^2)$ and $1/V_{appl}$ at the higher electric field (Figure 5b), indicating that the FE currents and applied voltages mostly followed the F−N law. The estimated values of β and S are listed in Table 2. Interestingly the NTNH emitters showed the largest β and the smallest S values. The largest β value of NTNH emitters was mainly due to the small diameters and the sparse distribution of SWNT bundles, which is recognized from the SEM image of the NTNH cathode (Figure 6a). In fact, it is well-known that the ideal ratio of the distance between the adjacent tubes to the tube height is about two by theoretical calculations.[45] On the other hand, the bundle diameters of HiPco-SWNTs (10−100 μm, Figure 6c) and HiPco-SWNTs/SWNHs (mainly 10−80 μm, Figure 6d) in the cathodes took various larger values, which might have caused the small values of β. The small β value of the SWNH emitter (Figure 6b) would be due to the small aspect ratio of individual SWNHs (diameter, 2−5 nm; length, 80−100 nm) and their high density. The *J*−*E* relation did not substantially depend on the amount of HiPco-SWNHs and the HiPco-SWNT/SWNH ratio (see Supporting Information Figure S6).

TABLE 2. Turn-on Electric Field, Field Enhancement Factors (β), and Effective Electron-Emission Area of Cathode Electrode (S) for Emitters Prepared Using NTNHs, HiPco-SWNTs, SWNHs, and HiPco-SWNTs/SWNHs (a Mixture of SWNTs and SWNHs)

	NTNH	SWNH	SWNT	SWNT/SWNH
turn-on electric field (kV/cm)	5	19	8.5	12
10^5 (cm^{-1})	2.50	0.56	1.2	0.79
S 10^6 (cm^2)	1.2	2.2	7.7	12.1

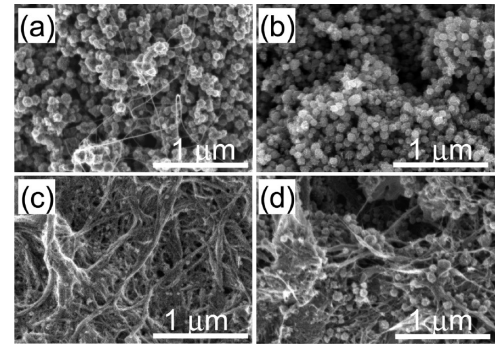

Figure 6. SEM images of cathode electrodes prepared using NTNHs (a), SWNHs (b), HiPco-SWNTs (c), HiPco-SWNTs/SWNHs (a mixture of SWNTs and SWNHs) (d), respectively.

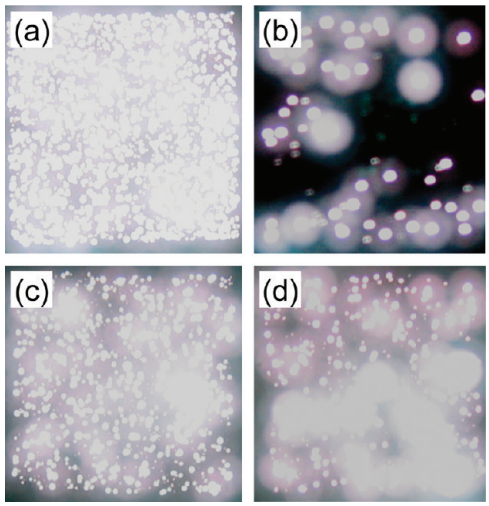

Figure 7. Photographs of light-emitting FELs prepared using NTNHs (a), SWNHs (b), HiPco-SWNTs (c), HiPco-SWNTs/SWNHs (a mixture of SWNTs and SWNHs) (d) at 14, 20, 14, and 14 kV/cm, respectively.

The NTNH-FEL having a small *S* value was homogeneously bright (Figure 7a), while the other FELs having larger *S* values showed quite patchy light emission (Figure 7b−d). Therefore, we think that large *S* values and homogeneous brightness may not be directly related.

The NTNH emitters had excellent electron emission efficiency (=large β value) from the thin-bundles of SWNTs that were few (=small *S* value) but homogeneously dispersed. The emitters using HiPco-SWNTs had low electron emission efficiency (=small β values) from thick bundles of which there were many (=large *S* values) but eccentrically localized on the electrodes. The SWNH-FEL cannot be the better emitter because of the small aspect ratio (=small β values) of SWNHs. The localized emission of SWNH-FEL (Figure 7b) could be attributed to summit-like morphologies on the cathode surface (Figure 6b).

CONCLUSIONS

To obtain a highly efficient field emission lamps (FELs) using single-walled carbon nanotubes (SWNTs), we hybridized SWNTs and single-walled carbon nanohorns (SWNHs) by growing SWNTs from Fe-catalyst supported on SWNHs by chemical vapor deposition. In the obtained SWNT-SWNH hybrids (NTNHs), the SWNT diameters were 1−1.7 nm and the bundle diameters were less than 10 nm. The FEL with the NTNH cathodes prepared by screen-printing showed the low electron emission threshold, 5 kV/cm, and homogeneous illumination from fluorescent materials deposited on the anode, owing to the small diameters of the SWNT bundles and their sparse and homogeneous distribution on the cathode. The high FE ability of SWNTs and high dispersion ability of SWNHs have been successfully combined in this NTNH-hybrid FEL.

MATERIALS AND METHODS

SWNH aggregates were prepared by CO_2 laser ablation of graphite rods,[21,22] and the holes were opened by heat treatment in dry air where the temperature was increased from room temperature to 500 °C at a rate of 1 °C/min (NHox).[30] Fe acetate (50 mg) and NHox (50 mg) were dispersed in ethanol (20 mL) and stirred at room temperature for about 12 h. The mixture was filtered, and black powder was obtained on the filter paper. The black powder was washed with ethanol (20 mL) once to remove the excess Fe acetate existing outside the NHox, and then dried for 24 h in vacuum at 80 °C (Fe@NHox).[31] The Fe@NHox was prebaked at 300 °C for 10 min in air (760 Torr) (Fe@NHoxh) to pyrolyze the Fe acetate to Fe oxide.[31] The resultant black powder was placed on a quartz boat located at the center of a reactor tube in an electric furnace, and the catalysts were reduced in the CVD reactor at 400 °C for 20 min in H_2(20%)/Ar(80%) flowing at 500 mL/min. Then, the flowing gas was changed from H_2/Ar to Ar and the temperature was increased to the desired CNT growth temperatures (600−1000 °C). After reaching the target temperature, the gas flow was switched to ethanol vapor, a carbon feedstock,[32] diluted in Ar, and kept for 15 min (NTNH). After the reaction, the reactor was cooled to room temperature in the Ar gas flow.

The structures of the specimens were observed with a transmission electron microscope (TEM) (Topcon EM-002B), scanning transmission electron microscope (STEM) (Hitachi HD-2300), and scanning electron microscope (SEM) (Hitachi S-4800). The TEM and STEM were operated at 120 kV, and the SEM was operated at 1.0 kV. Raman spectra were measured with a JASCO NRS-2000 Laser Raman spectrophotometer. The excitation wavelength of the Ar ion laser was 488 nm.

The obtained NTNH (50 mg) was mixed with ethyl-cellulose (100 mg), glass frit (200 mg), and α-terpineol (10 mL), and sufficiently stirred with roll-milling for about 6 h. The NTNH paste was screen-printed on an indium tin oxide (ITO) glass substrate (2 × 2 cm^2) through 400 mesh net. The NTNH paste/ITO was first dried at 80 °C in air, and then sintered at 500 °C in N_2 mainly to remove organic materials in the paste and to fix the granulous materials. The obtained NTNH/ITO (cathode) was put under a fluorescent plate (anode) at a distance of 1 mm, and an NTNH flat FEL was obtained. The NTNH FEL was placed in a vacuum chamber (1×10^{-7} Torr, room temperature), and the electrical properties (emission current *vs* applied voltage) and light emission from the fluorescent plates were tested. These FE properties of NTNHs were compared with those of HiPco-SWNTs, a mixture of HiPco-SWNTs and SWNHs (HiPco-SWNTs/SWNHs), and SWNHs only. The HiPco-SWNTs were purchased from Carbon Nanotechnologies, Inc. (diameter, 0.8−1.2 nm, see Supporting Information Figure S7). In HiPco-SWNTs/SWNHs, the weight ratio of HiPco-SWNTs and SWNHs was 1:1. The flat FEL devices from these three specimens were prepared in the same way as shown above for the NTNH devices, and the FE properties were similarly measured.

Acknowledgment. This work was in part performed under the management of the Nano Carbon Technology project supported by NEDO.

Supporting Information Available: Photograph and dynamic light scattering (DLS) results of SWNHs well dispersed in ethanol (Figure S1); TEM images of NTNHs prepared at 600 and 1000 °C (Figure S2); histogram of bundle diameter distributions of NTNHs (Figure S3); DLS results of NTNH hybrid well-dispersed in ethanol (Figure S4); typical STEM image of NTNH prepared at 800 °C by ethanol CVD (Figure S5); *J*−*E* curves obtained from HiPco-SWNTs, HiPco-SWNTs/SWNHs (10%) (a mixture of SWNTs (10 wt %) and SWNHs (90 wt %)), and HiPco-SWNTs/SWNHs (50%), respectively (Figure S6); Raman spectrum of HiPco-SWNTs purchased from Carbon Nanotechnologies, Inc. (Figure S7). This material is available free of charge *via* the Internet at http://pubs.acs.org.

REFERENCES AND NOTES

1. Iijima, S. Helical Microtubules of Graphitic Carbon. *Nature* **1991**, *354*, 56–58.
2. Iijima, S.; Ichihashi, T. Single-Shell Carbon Nanotubes of 1-nm Diameter. *Nature* **1993**, *363*, 603–605.
3. Tans, S. J.; Verschueren, A. R. M.; Dekker, C. Room-Temperature Transistor Based on a Single Carbon Nanotube. *Nature* **1998**, *393*, 49–52.
4. Frank, S.; Poncharal, P.; Wang, Z. L.; Heer, W. A. Carbon Nanotube Quantum Resistors. *Science* **1998**, *280*, 1744–1746.
5. Rueckes, T.; Kim, K.; Joselevich, E.; Tseng, G. Y.; Cheung, C. L.; Lieber, C. M. Carbon Nanotube-Based Nonvolatile Random Access Memory for Molecular Computing. *Science* **2000**, *289*, 94–97.
6. Itkis, M. E.; Borondics, F.; Yu, A.; Haddon, R. C. Bolometric Infrared Photoresponse of Suspended Single-Walled Carbon Nanotube Films. *Science* **2006**, *312*, 413–416.
7. Stampfer, C.; Helbling, T.; Obergfell, D.; Schöberle, B.; Tripp, M. K.; Jungen, A.; Roth, S.; Bright, V. M.; Hierold, C. Fabrication of Single-Walled Carbon-Nanotube-Based Pressure Sensors. *Nano Lett.* **2006**, *6*, 233–237.
8. Thess, A.; Lee, R.; Nikolaev, P.; Dai, H.; Petit, P.; Robert, J.; Xu, C.; Lee, Y. H.; Kim, S. G.; Rinzler, A. G.; *et al*. Crystalline Ropes of Metallic Carbon Nanotubes. *Science* **1996**, *273*, 483–487.
9. Vigolo, B.; Pénicaud, A.; Coulon, C.; Sauder, C.; Pailler, R.; Journet, C.; Bernier, P.; Poulin, P. Macroscopic Fibers and Ribbons of Oriented Carbon Nanotubes. *Science* **2000**, *290*, 1331–1334.
10. Hull, R. V.; Li, L.; Xing, Y.; Chusuei, C. C. Pt Nanoparticle Binding on Functionalized Multiwalled Carbon Nanotubes. *Chem. Mater.* **2006**, *18*, 1780–1788.
11. Chen, J.; Wang, M.; Liu, B.; Fan, Z.; Cui, K.; Kuang, Y. Platinum Catalysts Prepared with Functional Carbon Nanotube Defects and Its Improved Catalytic Performance for Methanol Oxidation. *J. Phys. Chem. B* **2006**, *110*, 11775–11779.
12. Rinzler, A. G.; Hafner, J. H.; Nikolaev, P.; Nordlander, P.; Colbert, D. T.; Smalley, R. E.; Lou, L.; Kim, S. G.; Tománek, D. Unraveling Nanotubes: Field Emission from an Atomic Wire. *Science* **1995**, *269*, 1550–1553.
13. Heer, W. A.; Châtelain, A.; Ugarte, D. A Carbon Nanotube Field-Emission Electron Source. *Science* **1995**, *270*, 1179–1180.
14. Bonard, J. M.; Stöckli, T.; Noury, O.; Châtelain, A. Field Emission from Cylindrical Carbon Nanotube Cathodes: Possibilities for Luminescent Tubes. *Appl. Phys. Lett.* **2001**, *78*, 2775–2777.
15. Chen, J.; Liang, X. H.; Deng, S. Z.; Xu, N. S. Flat-Panel Luminescent Lamp Using Carbon Nanotube Cathodes. *J. Vac. Sci. Technol. B* **2003**, *21*, 1727–1729.
16. Hiraoka, T.; Yamada, T.; Hata, K.; Futaba, D. N.; Kurachi, H.; Uemura, S.; Yumura, M.; Iijima, S. Synthesis of Single- and Double-Walled Carbon Nanotubes Forests on Conducting Metal Foils. *J. Am. Chem. Soc.* **2006**, *128*, 13338–13339.
17. Zhao, B.; Futaba, D. N.; Yasuda, S.; Akoshima, M.; Yamada, T.; Hata, K. Exploring Advantages of Diverse Carbon Nanotube Forests with Tailored Structures Synthesized by Supergrowth from Engineered Catalysts. *ACS Nano* **2009**, *3*, 108–114.
18. Gao, B.; Yue, G. Z.; Qiu, Q.; Cheng, Y.; Shimoda, H.; Fleming, L; Zhou, O. Fabrication and Electron Field Emission Properties of Carbon Nanotube Films by Electrophoretic Deposition. *Adv. Mater.* **2001**, *13*, 1770–1773.
19. Li, J.; Lei, W.; Zhang, X.; Zhou, X.; Wang, Q.; Zhang, Y.; Wang, B. Field Emission Characteristic of Screen-Printed Carbon Nanotube Cathode. *Appl. Surf. Sci.* **2003**, *220*, 96–104.
20. Lee, Y. D.; Lee, H. J.; Han, J. H.; Yoo, J. E.; Lee, Y. H.; Kim, J. K.; Nahm, S.; Ju, B. K. Synthesis of Double-Walled Carbon Nanotubes by Catalytic Chemical Vapor Deposition and Their Field Emission Properties. *J. Phys. Chem. B* **2006**, *110*, 5310–5314.
21. Iijima, S; Yudasaka, M.; Yamada, R.; Bandow, S.; Suenaga, K.; Kokai, F.; Takahashi, K. Nano-Aggregates of Single-Walled Graphitic Carbon Nano-Horns. *Chem. Phys. Lett.* **1999**, *309*, 165–170.
22. Iijima, S. Carbon Nanotubes: Past, Present, And Future. *Phys. B* **2002**, *323*, 1–5.
23. Urita, K.; Seki, S.; Utsumi, S.; Noguchi, D.; Kanoh, H.; Tanaka, H.; Hattori, Y.; Ochiai, Y.; Aoki, N.; Yudasaka, M.; *et al*. Effects of Gas Adsorption on the Electrical Conductivity of Single-Wall Carbon Nanohorns. *Nano Lett.* **2006**, *6*, 1325–1328.
24. Urita, K.; Seki, S.; Tsuchiya, H.; Honda, H.; Utsumi, S.; Hayakawa, C.; Kanoh, H.; Ohba, T.; Tanaka, H.; Yudasaka, M.; *et al*. Mechanochemically Induced sp^3-Bond-Associated Reconstruction of Single-Wall Carbon Nanohorns. *J. Phys. Chem. C* **2008**, *112*, 8759–8762.
25. Yoshitake, T.; Shimakawa, Y.; Kuroshima, S.; Kimura, H.; Ichihashi, T.; Kubo, Y.; Kasuya, D.; Takahashi, K.; Kokai, F.; Yudasaka, M.; *et al*. Preparation of Fine Platinum Catalyst Supported on Single-Wall Carbon Nanohorns for Fuel Cell Application. *Phys. B* **2002**, *323*, 124–126.
26. Yuge, R.; Ichihashi, T.; Shimakawa, Y.; Kubo, Y.; Yudasaka, M.; Iijima, S. Preferential Deposition of Pt Nanoparticles inside Single-Walled Carbon Nanohorns. *Adv. Mater.* **2004**, *16*, 1420–1423.
27. Yang, C. M.; Kim, Y. J.; Endo, M.; Kanoh, H.; Yudasaka, M.; Iijima, S.; Kaneko, K. Nanowindow-Regulated Specific Capacitance of Supercapacitor Electrodes of Single-Wall Carbon Nanohorns. *J. Am. Chem. Soc.* **2007**, *129*, 20–21.
28. Murakami, T.; Ajima, K.; Miyawaki, J.; Yudasaka, M.; Iijima, S.; Shiba, K. Drug-Loaded Carbon Nanohorns: Adsorption and Release of Dexamethasone *in Vitro*. *Mol. Pharm.* **2004**, *1*, 399–405.
29. Zhang, M.; Murakami, T.; Ajima, K.; Tsuchida, K.; Sandanayaka, A. S. D.; Ito, O.; Iijima, S.; Yudasaka, M. Fabrication of ZnPc/Protein Nanohorns for Double Photodyamic and Hyperthermic Cancer Phototherapy. *Proc. Natl. Acad. Sci. U.S.A.* **2008**, *105*, 14773–14778.
30. Fan, J.; Yudasaka, M.; Miyawaki, J.; Ajima, K.; Murata, K.; Iijima, S. Control of Hole Opening in Single-Wall Carbon Nanotubes and Single-Wall Carbon Nanohorns Using Oxygen. *J. Phys. Chem. B* **2006**, *110*, 1587–1591.
31. Miyawaki, J.; Yudasaka, M.; Imai, H.; Yorimitsu, H.; Isobe, H.; Nakamura, E.; Iijima, S. *In Vivo* Magnetic Resonance Imaging of Single-Walled Carbon Nanohorns by Labeling with Magnetite Nanoparticles. *Adv. Mater.* **2006**, *18*, 1010–1014.
32. Maruyama, S.; kojima, R.; Miyauchi, Y.; Chiashi, S.; Kohno, M. Low-Temperature Synthesis of High-Purity Single-Walled Carbon Nanotubes from Alcohol. *Chem. Phys. Lett.* **2002**, *360*, 229–234.
33. Saito, R.; Dresselhaus, G.; Dresselhaus, M. S. Trigonal Warping Effect of Carbon Nanotubes. *Phys. Rev. B* **2000**, *61*, 2981–2990.
34. Jorio, A.; Saito, R.; Hafner, J. H.; Lieber, C. M.; Hunter, M.; McClure, T.; Dresselhaus, G.; Dresselhaus, M. S. Structural (*n*, *m*) Determination of Isolated Single-Wall Carbon Nanotubes by Resonant Raman Scattering. *Phys. Rev. Lett.* **2001**, *86*, 1118–1121.
35. Dai, H.; Rinzler, A. G.; Nikolaev, P.; Thess, A.; Colbert, D. T.; Smalley, R. E. Single-Wall Nanotubes Produced by Metal-Catalyzed Disproportionation of Carbon Monoxide. *Chem. Phys. Lett.* **1996**, *260*, 471–475.
36. Cheung, C. L.; Kurtz, A.; Park, H.; Lieber, C. M. Diameter-Controlled Synthesis of Carbon Nanotubes. *J. Phys. Chem. B* **2002**, *106*, 2429–2433.
37. Bonard, J. M.; Chauvin, P.; Klinke, C. Monodisperse Multiwall Carbon Nanotubes Obtained with Ferritin as Catalyst. *Nano Lett.* **2002**, *2*, 665–667.
38. Fowler, R. H.; Hordheim, L. W. Electron Emission in Intense Electric Fields. *Proc. R. Soc. London, A* **1928**, *119*, 173–181.
39. Brodie, I.; Spindt, C. A. Vacuum Microelectronics. *Adv. Electron. Electron Phys.* **1992**, *83*, 1–106.
40. Nilsson, L.; Groening, O.; Groening, P.; Kuettel, O.;

Schlapbach, L. Characterization of Thin Film Electron Emitters by Scanning Anode Field Emission Microscopy. *J. Appl. Phys.* **2001**, *90*, 768–780.
41. Bonard, J. M.; Salvetat, J. P.; Stöckli, T.; Heer, W. A.; Forró, L.; Châtelain, A. Field Emission from Single-Wall Carbon Nanotube Films. *Appl. Phys. Lett.* **1998**, *73*, 918–920.
42. Sveningsson, M.; Morjan, R. E.; Nerushev, O. A.; Sato, Y.; Bäckström, J.; Campbell, E. E. B.; Rohmund, F. Raman Spectroscopy and Field-Emission Properties of CVD-Grown Carbon-Nanotube Films. *Appl. Phys. A: Mater. Sci. Process.* **2001**, *73*, 409–418.
43. Bonard, J. M.; Gaál, R.; Garaj, S.; Thien-Nga, L.; Forró, L.; Takahashi, K.; Kokai, F; Yudasaka, M.; Iijima, S. Field Emission Properties of Carbon Nanohorn Films. *J. Appl. Phys.* **2002**, *91*, 10107–10109.
44. Bonard, J. M.; Weiss, N.; Kind, H.; Stöckli, T.; Forró, L.; Kern, K.; Châtelain, A. Tuning the Field Emission Properties of Patterned Carbon Nanotube Films. *Adv. Mater.* **2001**, *13*, 184–188.
45. Nilsson, L.; Groening, O.; Emmenegger, C.; Kuettel, O.; Schaller, E.; Schlapbach, L.; Kind, H.; Bonard, J. M.; Kern, K. Scanning Field Emission from Paterned Carbon Nanotube Films. *Appl. Phys. Lett.* **2000**, *76*, 2071–2073.